Ultrashort-pulse second-harmonic generation with longitudinally nonuniform quasi-phase-matching gratings: pulse compression and shaping

G. Imeshev, M. A. Arbore,* and M. M. Fejer

E. L. Ginzton Laboratory, Stanford University, Stanford, California 94305

A. Galvanauskas, M. Fermann, and D. Harter

IMRA America, 1044 Woodridge Avenue, Ann Arbor, Michigan 48105

Received April 5, 1999; revised manuscript received August 16, 1999

We present a theory of ultrashort-pulse second-harmonic generation (SHG) in materials with longitudinally nonuniform quasi-phase-matching (QPM) gratings. We derive an expression for the output second-harmonic field generated in an arbitrary QPM grating from an arbitrary fundamental field, valid for arbitrary material dispersion in the undepleted-pump approximation. In the case when group-velocity dispersion can be neglected, a simple transfer-function relationship describes the SHG process. This SHG transfer function depends only on material properties and on the QPM grating design. We use this SHG transfer function to show that nonuniform QPM gratings can be designed to generate nearly arbitrarily shaped second-harmonic output pulses. We analyze in detail a technologically important example of pulse shaping: the generation of compressed second-harmonic pulses from linearly chirped fundamental input pulses. The efficiency of these interactions as well as the limits imposed by higher-order material dispersion are discussed. © 2000 Optical Society of America [S0740-3224(00)00401-X]

OCIS codes: 140.7090, 190.7110, 190.2620, 190.4360, 230.4320, 320.5520, 320.5540, 320.7110, 320.7080.

1. INTRODUCTION

Ultrashort-pulse lasers are very useful light sources for diverse applications, such as precision machining, multiphoton microscopy, ophthamological surgery, time-division-multiplexed communications, and time-domain spectroscopy. Nonlinear optical frequency conversion can be used to extend the useful wavelength range of available laser sources, in particular, ultrafast lasers. However, in many cases, inadequate properties of conventional nonlinear materials have prevented the application of frequency conversion to low-power sources. Recent advances in nonlinear materials, particularly that of the quasi-phase-matching (QPM) technique, have enabled the generation of an increasing range of wavelengths with improved efficiencies and with lower-power pump lasers.[1]

There has been substantial work on the theory of ultrashort-pulse nonlinear frequency conversion. Early experimental[2] and theoretical work[3,4] identified and quantified the group-velocity effects in second-harmonic generation (SHG) of ultrashort pulses. Akhmanov and co-workers wrote several reviews of the work in the field.[5–7] More recent work by Weiner[8,9] and by Sidick and co-workers[10–13] introduced the filter-function approach for description of ultrafast SHG in uniform crystals[8,9,11,12,14] and in uniform QPM gratings[13,14] as well as considered effects of higher-order dispersion.[11,14]

For nonlinear frequency conversion to be efficient, it is necessary that the phase velocities of the interacting waves be matched.[15] Conventional nonlinear materials rely on natural birefringence to attain this phase-velocity matching, limiting the choices of materials and polarizations that can be used for frequency conversion. A nonzero phase mismatch limits the interaction length to the distance, called the coherence length, over which the interacting waves acquire a π relative phase shift. With QPM[15,16] frequency conversion, the phase mismatch between the nonlinear polarization (generated by the input field/s) and the generated field is reset every coherence length by use of a spatial modulation of the nonlinear coefficient. The modulation period, Λ_0, is then chosen to be twice the coherence length. In terms of the k vectors of the interacting waves, the k vector of the periodic grating, $K = 2\pi/\Lambda_0$, must be equal to the k-vector mismatch of the interacting waves.

QPM allows for interactions between any combination of wavelengths within the transparency range of a material, allows use of nonbirefringent materials, and eliminates constraints on polarization, thereby enabling use of the large nonlinear coefficients available for interactions between parallel electric fields. QPM also provides extra degrees of freedom in engineering nonlinear interactions, which are not available with conventional birefringent phase matching. Although uniform periodic modulation of the nonlinearity is typically used for QPM, nonuniform modulation can also be desirable for tailoring the frequency response of a nonlinear device.

QPM interactions with longitudinally nonuniform gratings have been studied both theoretically and experimentally.[17–23] However, most treatments to date have considered the case of tunable cw SHG, rather than

ultrashort-pulse SHG. In previous work the phase response of nonuniform QPM gratings, critical to ultrashort-pulse interactions, was typically ignored. Engineering of the phase response was considered by Arbore *et al.*,[24] who proposed compression of ultrashort pulses during SHG in chirped QPM gratings that relied on the combination of spatial localization of conversion and group-velocity mismatch between the first-harmonic (FH) and the second-harmonic (SH) pulses. In that work the QPM-SHG process was analyzed assuming the undepleted pump approximation and negligible group-velocity dispersion (GVD) at both the FH and the SH wavelengths. It was shown that under these assumptions QPM-SHG can be described with a transfer-function formalism, relating the SH spectrum to the spectrum of the square of the FH pulse. This QPM-SHG transfer function depends only on intrinsic material properties and on the QPM grating design. Less-general forms of this transfer function were derived previously for particular cases of uniform crystals[4,8,11] and uniform QPM gratings.[13,14]

An experimental demonstration of pulse compression during SHG in chirped-period-poled lithium niobate was presented in Ref. 25. The effects of GVD, which were not included in the available theory, were proposed as the origin of small discrepancies between theoretical expectations and experimental observations, which was shown to be the case in Ref. 26. The use of chirped QPM gratings in practical laser systems has also been demonstrated.[27–30] Engineerable shaping of complex pulses during SHG with Fourier synthetic QPM gratings was proposed and demonstrated in Ref. 31.

In this paper we develop the theory of ultrafast SHG with longitudinally nonuniform QPM gratings in the undepleted pump approximation and extend the theoretical framework of Ref. 24 to include material dispersion beyond GVM. This paper is organized as follows. Section 2 presents an intuitive time-domain picture of ultrashort-pulse SHG as well as pulse compression and shaping with nonuniform QPM gratings by emphasizing the importance of the GVM effect (intrinsic material property) and spatial localization of conversion (engineerable property of a QPM grating). Section 3 presents a rigorous treatment of the ultrashort-pulse SHG process. A frequency-domain analysis is used because it allows convenient inclusion of arbitrary material dispersion properties. We derive a general result that is not a transfer function in nature but applies in the case of arbitrary material dispersion and pulse length. Neglecting GVD at both FH and SH frequencies, in Section 4 we rederive the simple transfer-function relationship of Ref. 24. Inclusion of GVD and higher-order dispersion terms at the SH frequency still produces a transfer-function result and hence can easily be accounted for. GVD at the FH leads to a result that cannot be expressed in terms of a transfer function; however, for a given FH pulse shape, GVD still can be accounted for in a straightforward manner. Detailed analytic treatment of GVD at both FH and SH frequencies will be described in a subsequent paper.

The remainder of the paper uses this transfer-function formalism. In Section 5 we consider the SHG process (both cw and pulsed) with uniform QPM gratings and rederive the well-known effects of GVM on the SH pulse length (Refs. 3, 4, 8, and 9). In Section 6 we show the utility of nonuniform QPM gratings for pulse shaping and give the explicit prescription for the grating design that will perform the necessary shaping function. A particular technologically important example of pulse shaping, pulse compression with linearly chirped QPM gratings, is analyzed in detail in Section 7. Scaling laws for the conversion efficiency of plane-wave and focused beams (Sections 8 and 9, respectively) are derived for uniform gratings as well as for a general QPM-SHG pulse shaper and in particular for a chirped-grating compressor. Section 10 is a comparison of several QPM materials in terms of their performance in ultrafast SHG devices. Finally, we summarize the results of this paper.

2. TIME-DOMAIN DESCRIPTION OF ULTRASHORT-PULSE SECOND-HARMONIC GENERATION, PULSE COMPRESSION, AND PULSE SHAPING

The envelope of an optical pulse propagates through a medium at a characteristic group velocity. In general, because of the material dispersion, the group velocity of the SH pulse envelope, u_2, is not the same as the group velocity of the FH pulse envelope, u_1. This group-velocity mismatch (GVM) leads to the group-velocity walk-off effect. When a transform-limited FH pulse propagates through the nonlinear medium, at each spatial position it generates a contribution to the SH field. Because of the GVM, the SH fields generated at different positions in the nonlinear medium undergo different time delays relative to the FH pulse as observed at the output of the material. The characteristic length over which FH and SH pulses walk off each other is called the group-velocity walk-off length, $L_{gv} = \tau_1/|\delta\nu|$, where τ_1 is the FH pulse length and $\delta\nu = 1/u_1 - 1/u_2$ is the GVM parameter. When the length of the nonlinear crystal exceeds L_{gv}, a distorted SH pulse with a length longer than τ_1 typically results. Because GVM is a result of linear dispersive properties of the material, QPM, which modulates the nonlinear coefficient, does not qualitatively alter the situation described above.

Pulse shaping and pulse compression with nonuniform QPM gratings can be explained as a result of the interplay of two phenomena: GVM between the FH and SH pulses, intrinsic to the nonlinear material, and spatial localization of SH conversion of particular frequency components, an engineerable property of QPM gratings. As discussed above, GVM maps the position of the QPM grating to time delay between FH and SH pulses. The local grating period determines which wavelength can be doubled. Therefore in a nonuniform grating, different spatial regions of the nonlinear material quasi-phase-match doubling of different frequency components of the FH pulse. In other words, nonuniform QPM maps position in the grating onto the frequency components of a pulse. Together, these phenomena map frequency to time delay.

Let us consider in more detail how a chirped QPM grating can impose an additional effective GVD on the SH pulse. Figure 1 shows the evolution of two different spec-

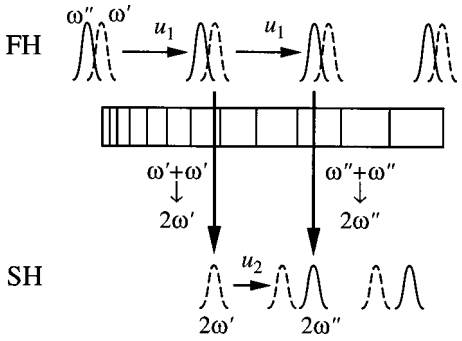

Fig. 1. Time-domain picture of SHG with a chirped QPM grating. Two different spectral components of the FH pulse, ω' (dashed curve) and ω'' (solid curve) propagate through the crystal with the same group velocity u_1. At a certain position in the grating determined by the local QPM period the FH component ω' generates the SH component $2\omega'$ (dashed curve), which then freely travels to the end of the crystal with group velocity $u_2 \neq u_1$. The other FH component, ω'', gets converted to SH component $2\omega''$ (solid curve) further in the crystal, and then this SH component travels with group velocity u_2. Because $u_2 \neq u_1$, the $2\omega'$ and $2\omega''$ components acquire a particular time delay relative to each other and to the FH pulse.

tral components of the FH pulse, ω' and ω'', and the SH pulse, $2\omega'$ and $2\omega''$, in a chirped QPM grating. In the absence of material GVD, both frequency components of the FH pulse travel through the crystal with the same group velocity u_1 to the position in the crystal where the local QPM period is appropriate for conversion of the FH pulse component at ω' into the corresponding SH frequency component $2\omega'$. This SH component then freely travels to the end of the crystal with group velocity $u_2 \neq u_1$. The other FH component, ω'', gets converted to SH component $2\omega''$ further in the crystal, and then this SH component travels with group velocity u_2. Because of the GVM the $2\omega'$ and $2\omega''$ components of the generated SH pulse acquire a particular time delay relative to each other and to the FH pulse. Strictly speaking, this is an oversimplified picture because the conversion is driven by the square of the FH pulse, and hence we have to consider propagation of the frequency components of the square of the FH pulse. This distinction becomes important in the case when material GVD is nonnegligible, as will be shown by the frequency-domain analysis, quantified in Eq. (24), and addressed in detail in a subsequent paper.

We now consider pulse compression with a chirped grating. Let FH be a chirped pulse, i.e., a pulse whose spectral components are delayed with respect to each other. By appropriate choice of the locations in the grating where each component of the FH generates the corresponding SH component, the relative delay of the SH pulse components owing to the grating chirp can be made equal and opposite to that from the chirp of the FH pulse. The net relative delay will then be zero; i.e., the SH will be compressed.

It is clear from this time-domain argument that the chirped QPM grating must be at least as long as the temporal walk-off length. This minimum material length arises from the need for the SH pulse to walk through the entire FH pulse, picking up frequency components along its way. We note that although the conversion process for a particular frequency component happens over some finite length, not at a localized point, this time-domain picture is still very useful for understanding the physics of the process. A more quantitative and rigorous frequency-domain analysis of these pulse compression and shaping phenomena is presented in the following sections.

3. FREQUENCY-DOMAIN TREATMENT OF ULTRAFAST SECOND-HARMONIC GENERATION

We begin the analysis with Maxwell's equations expressed in the frequency domain. We use the following notation: if $F(t)$ is a function of time, then $\hat{F}(\omega)$ is its temporal Fourier transform, where ω represents optical radian frequencies. We use the transform pair

$$F(t) \equiv \int_{-\infty}^{+\infty} \hat{F}(\omega)\exp(i\omega t)\mathrm{d}\omega, \tag{1}$$

$$\hat{F}(\omega) \equiv \frac{1}{2\pi}\int_{-\infty}^{+\infty} F(t)\exp(-i\omega t)\mathrm{d}t, \tag{2}$$

and Maxwell's equations are thus written in the form

$$\nabla \times \hat{\mathbf{E}}(\mathbf{r}, \omega) = -i\omega\hat{\mathbf{B}}(\mathbf{r}, \omega), \tag{3}$$

$$\nabla \times \hat{\mathbf{H}}(\mathbf{r}, \omega) = i\omega\hat{\mathbf{D}}(\mathbf{r}, \omega), \tag{4}$$

where $\hat{\mathbf{E}}(\mathbf{r}, \omega)$, $\hat{\mathbf{B}}(\mathbf{r}, \omega)$, $\hat{\mathbf{H}}(\mathbf{r}, \omega)$, and $\hat{\mathbf{D}}(\mathbf{r}, \omega)$ are the Fourier transforms of the full electric-field, magnetic-field, magnetic-displacement, and electric-displacement vectors, respectively. For nonmagnetic and nonlinear dielectrics we use the constitutive relations $\hat{\mathbf{B}}(\mathbf{r}, \omega) = \mu_0\hat{\mathbf{H}}(\mathbf{r}, \omega)$ and $\hat{\mathbf{D}}(\mathbf{r}, \omega) = \epsilon_0\epsilon(\omega)\hat{\mathbf{E}}(\mathbf{r}, \omega) + \hat{\mathbf{P}}_{\mathrm{NL}}(\mathbf{r}, \omega)$, where $\hat{\mathbf{P}}_{\mathrm{NL}}(\mathbf{r}, \omega)$ is the electric nonlinear polarization component at frequency ω, $\epsilon(\omega) = n^2(\omega)$ is the dielectric constant, and n is the refractive index. We assume lossless, isotropic, nongyrotropic media so that $\mathbf{D}(\mathbf{r}, t)$ is parallel to $\mathbf{E}(\mathbf{r}, t)$, and ϵ is a real scalar quantity.

For the case of SHG, assuming that the FH and the SH spectra do not overlap, we decompose the full electric field into a sum of components at the FH, $\hat{\mathbf{E}}_1$, and the SH, $\hat{\mathbf{E}}_2$, frequencies, $\hat{\mathbf{E}}(\mathbf{r}, \omega) = \hat{\mathbf{E}}_1(\mathbf{r}, \omega) + \hat{\mathbf{E}}_2(\mathbf{r}, \omega)$. Assuming plane-wave interactions with an undepleted pump and propagation direction z, from Eqs. (3) and (4) we obtain the following pair of coupled one-dimensional frequency-domain scalar wave equations:

$$\frac{\partial^2}{\partial z^2}\hat{E}_1(z, \omega) + k^2(\omega)\hat{E}_1(z, \omega) = 0, \tag{5}$$

$$\frac{\partial^2}{\partial z^2}\hat{E}_2(z, \omega) + k^2(\omega)\hat{E}_2(z, \omega) = -\mu_0\omega^2\hat{P}_{\mathrm{NL}}(z, \omega), \tag{6}$$

where the k vector in the medium is $k^2(\omega) = \omega^2\epsilon(\omega)/c^2$.

In a medium that is negligibly dispersive in $\chi^{(2)}$ the nonlinear polarization spectrum, $\hat{P}_{\mathrm{NL}}(z, \omega)$, which drives the SH conversion, can be written in terms of the FH electric field in the form[32]

$$\hat{P}_{\mathrm{NL}}(z,\omega) = \frac{1}{2}\epsilon_0\chi^{(2)}(z)\int_{-\infty}^{+\infty}\hat{E}_1(z,\omega')\hat{E}_1(z,\omega-\omega')\mathrm{d}\omega', \tag{7}$$

where $\chi^{(2)}(z)$ is the material nonlinear susceptibility, allowed here to vary with position. We now define a position-dependent (modulated) nonlinear coefficient, $d(z)$, such that $\chi^{(2)}(z) \equiv 2d(z)$. We note that with $d(z)$ defined in this way, Eq. (7) corresponds to the simple time-domain relation $P_{\mathrm{NL}}(z,t) = \epsilon_0 d(z)E_1^2(z,t)$.

Optical signals most generally described by a time- and position-dependent electric field, $E(z,t)$, are usually represented by an envelope function. The typical envelope definition used in the nonlinear optics literature (see, for example, Ref. 33) for pulsed optical fields is defined in the time domain, with the optical carrier frequency ω_i and k vector $k_i \equiv k(\omega_i)$ explicitly factored out (here and in the rest of the paper the subscript $i = 1$ denotes the FH and $i = 2$ denotes the SH). This time-domain envelope, $B_i(z,t)$, is related to the electric field by

$$E_i(z,t) = B_i(z,t)\exp(i\omega_i t - ik_i z). \tag{8}$$

The temporal Fourier transform of the electric field, $\hat{E}_i(z,\omega)$, is then related to the Fourier transform of this time-domain envelope, $\hat{B}_i(z,\Omega_i)$, as

$$\hat{E}_i(z,\omega) = \hat{B}_i(z,\Omega_i)\exp(-ik_i z), \tag{9}$$

where we introduced the frequency detunings $\Omega_2 = \omega - \omega_2 \equiv \Omega$ and $\Omega_1 = \omega - \omega_1$.

Though intuitive, this time-domain envelope leads to an unnecessarily complex analysis for the important case of SHG in materials with nonnegligible GVD and higher-order dispersion. Rather, for the derivation presented in this paper, we define a frequency-domain spatial envelope, $\hat{A}_i(z,\Omega_i)$, such that the Fourier transform of the electric field can be written in the form

$$\hat{E}_i(z,\omega) = \hat{A}_i(z,\Omega_i)\exp[-ik(\omega_i+\Omega_i)z]. \tag{10}$$

This definition leads to a mathematically and physically transparent analysis because it explicitly describes the effect of material dispersion on each frequency component of the interacting waves, as we will see more clearly later in the paper. Comparing Eqs. (9) and (10), we obtain the relation between the two envelopes:

$$\hat{B}_i(z,\Omega_i) = \hat{A}_i(z,\Omega_i)\exp\{-i[k(\omega_i+\Omega_i)-k_i]z\}. \tag{11}$$

We note that at $z = 0$, as well as for $\Omega_i = 0$, the frequency-domain envelope and the Fourier transform of the time-domain envelope are equal to each other; i.e.,

$$\hat{A}_i(0,\Omega_i) = \hat{B}_i(0,\Omega_i), \tag{12}$$

$$\hat{A}_i(z,0) = \hat{B}_i(z,0). \tag{13}$$

This envelope definition, Eq. (10), reduces to that of Ref. 8 in the limit of negligible GVD and higher-order dispersion.

Substituting the frequency-domain envelope definition, Eq. (10), into the coupled wave equations, Eqs. (5) and (6), and using the slowly varying envelope approximation, i.e., assuming that $\mathrm{d}^2\hat{A}_i/\mathrm{d}z^2 \ll k(\omega)(\mathrm{d}\hat{A}_i/\mathrm{d}z)$, we obtain

$$\frac{\partial}{\partial z}\hat{A}_1(z,\Omega_1) = 0, \tag{14}$$

$$\frac{\partial}{\partial z}\hat{A}_2(z,\Omega) = -i\frac{\mu_0\omega_2^2}{2k_2}\hat{P}_{\mathrm{NL}}(z,\Omega)\exp[ik(\omega_2+\Omega)z], \tag{15}$$

with the nonlinear polarization expressed with Eqs. (7) and (10) in terms of the FH envelope as

$$\hat{P}_{\mathrm{NL}}(z,\Omega) = \epsilon_0 d(z)\int_{-\infty}^{+\infty}\hat{A}_1(z,\Omega')\hat{A}_1(z,\Omega-\Omega') \times \exp\{-i[k(\omega_1+\Omega')+k(\omega_1+\Omega-\Omega')]z\}\mathrm{d}\Omega', \tag{16}$$

where $\Omega' \equiv \omega' - \omega_1$.

Equation (14) describes free propagation of the FH wave through a dispersive medium; its solution is

$$\hat{A}_1(z,\Omega) = \hat{A}_1(\Omega), \tag{17}$$

where $\hat{A}_1(\Omega) \equiv \hat{A}_1(z=0,\Omega)$ is the FH envelope at the input ($z = 0$) of the nonlinear crystal of length L. We note that because the effects of dispersion are explicitly retained in the definition of the frequency-domain envelope, Eq. (10), $\hat{A}_1$ is independent of position within the crystal, even though the FH experiences dispersion, as we can see by writing the FH electric field, Eq. (10), with Eq. (17):

$$\hat{E}_1(z,\omega) = \hat{A}_1(\Omega)\exp[-ik(\omega_1+\Omega)z]. \tag{18}$$

Substituting the solution for the FH envelope, Eq. (17), into the expression for $\hat{P}_{\mathrm{NL}}(z,\Omega)$, Eq. (16), we obtain the output SH envelope by integrating Eq. (15):

$$\hat{A}_2(L,\Omega) = \int_{-\infty}^{+\infty}\hat{A}_1(\Omega')\hat{A}_1(\Omega-\Omega')\hat{d}[\Delta k(\Omega,\Omega')]\mathrm{d}\Omega', \tag{19}$$

where we defined the k-vector mismatch as

$$\Delta k(\Omega,\Omega') = k(\omega_1+\Omega') + k(\omega_1+\Omega-\Omega') - k(\omega_2+\Omega), \tag{20}$$

and $\hat{d}[\Delta k(\Omega,\Omega')]$ is proportional to the spatial Fourier transform of $d(z)$, with $\Delta k(\Omega,\Omega')$ serving as the transform variable:

$$\hat{d}(\Delta k) = -i\gamma\int_{-\infty}^{+\infty}d(z)\exp(-i\Delta k z)\mathrm{d}z, \tag{21}$$

where $\gamma \equiv 2\pi/(\lambda_1 n_2)$, λ_1 is the free-space FH wavelength, and n_2 is the refractive index at the SH frequency. In writing Eqs. (19)–(21) we assumed no SH field input to the crystal and we increased the integration bounds in Eq. (21) from $[0, L]$ to $(-\infty, +\infty)$, recognizing that this cannot affect the solution because $d(z) = 0$ outside of the crystal.

With Eqs. (19)–(21) one can find the output SH envelope $\hat{A}_2$ given the input FH envelope $\hat{A}_1$, the dispersive properties of the medium, represented by the functional dependence $\Delta k = \Delta k(\Omega,\Omega')$, and the modulated nonlin-

ear coefficient $d(z)$. We note that Eqs. (19)–(21) are valid for materials with arbitrary dispersion or, equivalently, for the FH and the SH pulses with arbitrarily broad nonoverlapping spectra. Assuming that the frequency detunings are small compared with the carrier frequencies, i.e., $\Omega,\Omega' \ll \omega_1,\omega_2$, we perform a Taylor expansion of Eq. (20), resulting in

$$\Delta k(\Omega, \Omega') = \Delta k'(\Omega) + \Delta k''(\Omega, \Omega'), \tag{22}$$

with

$$\Delta k'(\Omega) = \Delta k_0 + \delta\nu\Omega + \frac{1}{2}\delta\beta\Omega^2 + \delta k'(\Omega), \tag{23}$$

$$\Delta k''(\Omega, \Omega') = \beta_1(\Omega'^2 - \Omega\Omega') + \delta k''(\Omega, \Omega'), \tag{24}$$

where $\Delta k_0 = 2k_1 - k_2$ is the carrier k-vector mismatch, $\delta\nu = 1/u_1 - 1/u_2$ is the GVM parameter with $u_i \equiv [\mathrm{d}k(\omega)/\mathrm{d}\omega]^{-1}|_{\omega=\omega_i}$ being the group velocities, and $\delta\beta = \beta_1 - \beta_2$ is the GVD mismatch parameter with $\beta_i \equiv [\mathrm{d}^2k(\omega)/\mathrm{d}\omega^2]|_{\omega=\omega_i}$ being the GVD parameters. The remainder terms $\delta k'(\Omega)$ and $\delta k''(\Omega, \Omega')$ are of the order of Ω^3 and Ω'^3. Note that in the ultrafast literature it is common to use β_2 for the GVD coefficient of the dispersive material at a particular wavelength. Here, however, for notational simplicity we use β_i for the GVD coefficient with the subscript referring to either the FH or the SH.

4. TRANSFER-FUNCTION INTERPRETATION OF SECOND-HARMONIC GENERATION

For the rest of the paper we will assume that GVD and higher-order dispersion terms at the FH and SH wavelengths can be ignored. The length of a transform-limited pulse, τ_β, for which GVD becomes important in a crystal of length L, is defined by $\tau_\beta{}^2 = L|\beta|$. The results presented in the rest of this paper are valid for pulses longer than this limit set by the GVD. Inclusion of GVD leads to a more complicated analysis as briefly discussed in the conclusion; this inclusion of GVD will be the subject of a subsequent paper, for which the set of Eqs. (19) and (21)–(24) will be a starting point of the analysis.

Explicitly, if the GVD parameters $\beta_1 = \beta_2 = 0$ and the remainder terms $\delta k'(\Omega) = \delta k''(\Omega, \Omega') = 0$, then $\Delta k'(\Omega) = \Delta k_0 + \delta\nu\Omega$ in Eq. (23) and $\Delta k''(\Omega, \Omega') = 0$ in Eq. (24), and hence $\hat{d}[\Delta k(\Omega, \Omega')]$, as defined by Eq. (21), becomes Ω' independent. We define a new notation for this special case, $\hat{D}(\Omega) \equiv \hat{d}(\Delta k_0 + \delta\nu\Omega)$, or, with Eq. (21),

$$\hat{D}(\Omega) = -i\gamma\int_{-\infty}^{+\infty} d(z)\exp[-i(\Delta k_0 + \delta\nu\Omega)z]\mathrm{d}z. \tag{25}$$

Because $\hat{D}(\Omega)$ is independent of Ω', it can be factored out from under the integral in Eq. (19), resulting in

$$\hat{A}_2(L, \Omega) = \hat{D}(\Omega)\widehat{A_1^2}(\Omega), \tag{26}$$

where $\widehat{A_1^2}(\Omega)$ is a self-convolution of $\hat{A}_1(\Omega)$:

$$\widehat{A_1^2}(\Omega) = \int_{-\infty}^{+\infty}\hat{A}_1(\Omega')\hat{A}_1(\Omega - \Omega')\mathrm{d}\Omega'. \tag{27}$$

According to the convolution theorem, $\widehat{A_1^2}(\Omega)$ defined by Eq. (27) is the Fourier transform of the square of $A_1(t)$. Taking the inverse Fourier transform of Eq. (26) we obtain the time-domain relation:

$$A_2(L, t) = -i\gamma[d(t/\delta\nu)\exp(-i\Delta k_0 t/\delta\nu)] \otimes A_1^2(t), \tag{28}$$

where $\otimes$ denotes convolution.

Equations (26) and (27) can be rewritten in terms of the conventional time-domain envelopes with Eqs. (11) and (12), resulting in

$$\hat{B}_2(L, \Omega) = \hat{D}(\Omega)\widehat{B_1^2}(\Omega)\exp(-i\Omega L/u_2), \tag{29}$$

with $\widehat{B_1^2}(\Omega)$ defined as

$$\widehat{B_1^2}(\Omega) = \int_{-\infty}^{+\infty}\hat{B}_1(z = 0, \Omega')\hat{B}_1(z = 0, \Omega - \Omega')\mathrm{d}\Omega'. \tag{30}$$

The extra phase factor in Eq. (29) as compared with Eq. (26) is linear in Ω and hence represents a simple shift in time, resulting from different definitions for the time- and frequency-domain envelopes.

In Eq. (26) the factor $\hat{D}(\Omega)$ is a transfer function that relates the spectrum of the SH envelope to the spectrum of the square of the FH. $\hat{D}(\Omega)$ is a generalized version of a transfer function derived previously for uniform QPM gratings.[13,14] $\hat{D}(\Omega)$ depends only on the dispersive properties of the medium and the modulated nonlinear coefficient distribution, but not on any of the input pulse parameters, and hence can be viewed as a filter function acting on the different spectral components of the FH pulse. This transfer function result is the basis for general pulse shaping and, in particular, pulse compression with QPM gratings. The time-domain picture of pulse shaping, outlined in Section 2, can be derived from these frequency-domain equations. In the time domain, pulse shaping with QPM gratings relies on the combination of the group-velocity walk-off effect and the spatial localization of the SHG process. Equation (25) states that for every frequency Ω, $\hat{D}(\Omega)$ is obtained by summing contributions from different sections of the QPM grating. Each contribution is offset by a phase that is linear in Ω. In the time domain this phase corresponds to a delay, whose value is determined by the longitudinal coordinate z and the GVM parameter $\delta\nu$, as indicated in Eq. (28).

5. UNIFORM QUASI-PHASE-MATCHING GRATINGS

In practice QPM gratings generally use binary modulation of the nonlinear coefficient, i.e., mathematically $d(z)$ is a square wave whose amplitude is the intrinsic nonlinear coefficient of the material, d_{eff}. The particular case of a uniform grating was analyzed previously[13,14]; in this section we rederive those results using the transfer-function formalism. For a uniform grating of constant period Λ_0, $d(z)$ can be decomposed into the spatial Fourier components $d_m(z)$ with k vectors $K_m = 2\pi m/\Lambda_0$,

$$d(z) = \sum_m d_m(z) = \sum_m |d_m|\exp(iK_m z), \tag{31}$$

where $|d_m|$ is the amplitude of the mth Fourier component of the grating, which is evaluated for a uniform square grating as[16]

$$|d_m| = \frac{2}{\pi m} d_{\text{eff}} \sin(\pi m G), \tag{32}$$

where G is the duty cycle of the grating. If $G = 0$, i.e., the material is unmodulated, then $|d_m| = 0$, which indicates that there is no modulated component of the QPM grating. The maximum value of $|d_m|$ is $(2/\pi m)d_{\text{eff}}$, which is achieved at $G = 0.5$ for an odd-order or at $G = 1/(2m)$ for an even-order QPM process, respectively.

Substituting Eq. (31) into Eq. (25), we find that only the Fourier component whose k vector is close to Δk_0, $K_m \approx \Delta k_0$, contributes significantly to $\hat{D}(\Omega)$, resulting in the following well-known expression for the uniform-grating transfer function[13,14]:

$$\hat{D}(\Omega) = \gamma L |d_m| \text{sinc}[(\Delta k_0 - K_m + \Omega \delta\nu)L/2], \tag{33}$$

where $\text{sinc}(x) \equiv \sin(x)/x$ and we neglect a linear-in-Ω phase factor, which corresponds in the time domain to a simple time delay. The width of this transfer function, $\Delta\Omega_g$, is determined by the GVM parameter $\delta\nu$ and scales inversely with the crystal length L: $\Delta\Omega_g \propto 1/(\delta\nu L)$.

Let us first consider the case of cw SHG with uniform QPM grating, i.e., the input FH field is a monochromatic wave with frequency $\omega_1 + \Omega_1$, where Ω_1 is the detuning from the nominal (in the sense of the envelope carrier) FH optical frequency, ω_1. Thus

$$E_1(z = 0, t) = E_1 \exp[i(\omega_1 + \Omega_1)t]. \tag{34}$$

The envelope self-convolution, Eq. (27), can be written as

$$\widehat{A_1^2}(\Omega) = E_1^2 \delta(\Omega - 2\Omega_1). \tag{35}$$

Substituting Eq. (35) into Eq. (26) and using the result of Eq. (33), we obtain the output SH envelope as

$$\hat{A}_2(L, \Omega_2 = 2\Omega_1) = E_1^2 \gamma L |d_m| \text{sinc}[(\Delta k_0 - K_m + \Omega_2 \delta\nu)L/2]. \tag{36}$$

The SH field described by the envelope of Eq. (36) is a monochromatic wave at frequency $\omega_2 + \Omega_2 = 2(\omega_1 + \Omega_1)$. The result of Eq. (36) gives the familiar sinc^2 tuning curve when its square magnitude is evaluated.

From Eq. (36) we obtain the well-known quasi-phase-matching condition for the SHG process[15,16]; i.e., the k vector of the grating should be equal to the k-vector mismatch of the interacting waves, or $K_m = \Delta k_0$. We note that this result is also valid for uniform unmodulated (non-QPM) materials, where $K_m = 0$ and hence the phase-matching condition is $\Delta k_0 = 0$.

We now consider the case of SHG pumped by a Gaussian FH pulse with optical carrier frequency ω_1, $1/e$ power half-width τ_0 and real (temporal peak) amplitude E_0. The time-domain envelope of the electric field that corresponds to this pulse is

$$B_1(0, t) = E_0 \exp\left(-\frac{t^2}{2\tau_0^2}\right). \tag{37}$$

Using the frequency-domain envelope definition, Eq. (10), we obtain $\hat{A}_1(\Omega)$ for this pulse as

$$\hat{A}_1(\Omega) = \frac{1}{\sqrt{2\pi}} E_0 \tau_0 \exp\left(-\frac{1}{2}\tau_0^2 \Omega^2\right). \tag{38}$$

The SH envelope is then obtained from Eq. (26), with the transfer function given by Eq. (33):

$$\hat{A}_2(\Omega) = \frac{\gamma}{2\sqrt{\pi}} E_0^2 L |d_m| \tau_0 \exp\left(-\frac{1}{4}\tau_0^2 \Omega^2\right) \text{sinc}(\Omega \delta\nu L/2), \tag{39}$$

where we assumed that the interaction is quasi phase matched, i.e., $K_m = \Delta k_0$.

The shape of the SH pulse depends on the ratio of the bandwidth of $\widehat{A_1^2}(\Omega)$, $\Delta\Omega$, and the acceptance bandwidth of the uniform grating, the width $\Delta\Omega_g$ of $\hat{D}(\Omega)$ given by Eq. (33), as can be seen from Eq. (39). Figure 2 shows $\widehat{A_1^2}(\Omega)$ and $\hat{D}(\Omega)$ for two representative cases of different ratios of these bandwidths. In the time domain, this bandwidth consideration can be restated: the shape of the SH pulse depends on the ratio of the crystal length L to the group-velocity walk-off length L_{gv}, defined as

$$L_{\text{gv}} = \frac{\tau_0}{|\delta\nu|}. \tag{40}$$

The temporal shape of the SH pulse can be obtained by the inverse Fourier transform of Eq. (39). We numerically evaluated the temporal $1/e$ power half-width of the SH pulse, τ_2, as a function of L/L_{gv}, with the results shown in Figs. 3(a) and 3(c).

In the quasi-stationary case, when the crystal length is short enough such that the walk-off effects are negligible, i.e., $L \ll L_{\text{gv}}$, the SH pulse profile is just the square of the Gaussian FH pulse and hence the SH pulse length is $\tau_2 = \tau_0/\sqrt{2}$. The condition $L \ll L_{\text{gv}}$ corresponds to the frequency-domain condition $\Delta\Omega_g \gg \Delta\Omega$, i.e., $\Delta\Omega_g$ is broad enough to accommodate conversion of all frequency components, such that the grating does not affect the shape of the SH.

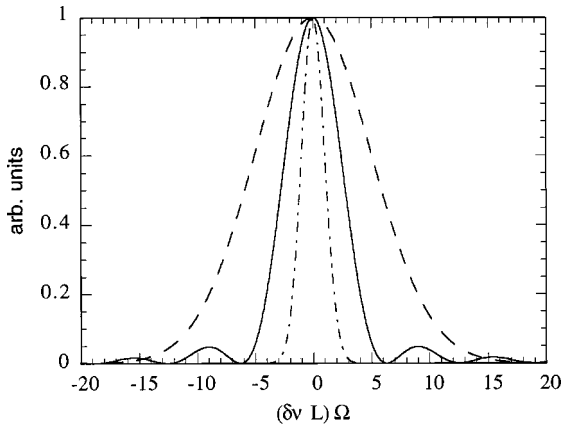

Fig. 2. Square of absolute value of the transfer function for the uniform grating, Eq. (33), $|\hat{D}(\Omega)|^2 \propto \text{sinc}^2(\Omega\delta\nu L/2)$ (solid curve) and the square of the absolute value of $\widehat{A_1^2}(\Omega)$ for a Gaussian FH pulse, Eq. (37), $|\widehat{A_1^2}(\Omega)|^2 \propto \exp(-\tau_0^2\Omega^2/4)$ for $\tau_0 = \delta\nu L$ such that $L/L_{\text{gv}} = 1$ (dash-dotted curve) and $\tau_0 = 0.2\delta\nu L$ such that $L/L_{\text{gv}} = 5$ (dashed curve). $|\hat{D}(\Omega)|^2$ and $|\widehat{A_1^2}(\Omega)|^2$ are plotted as functions of normalized frequency $(\delta\nu L)\Omega$.

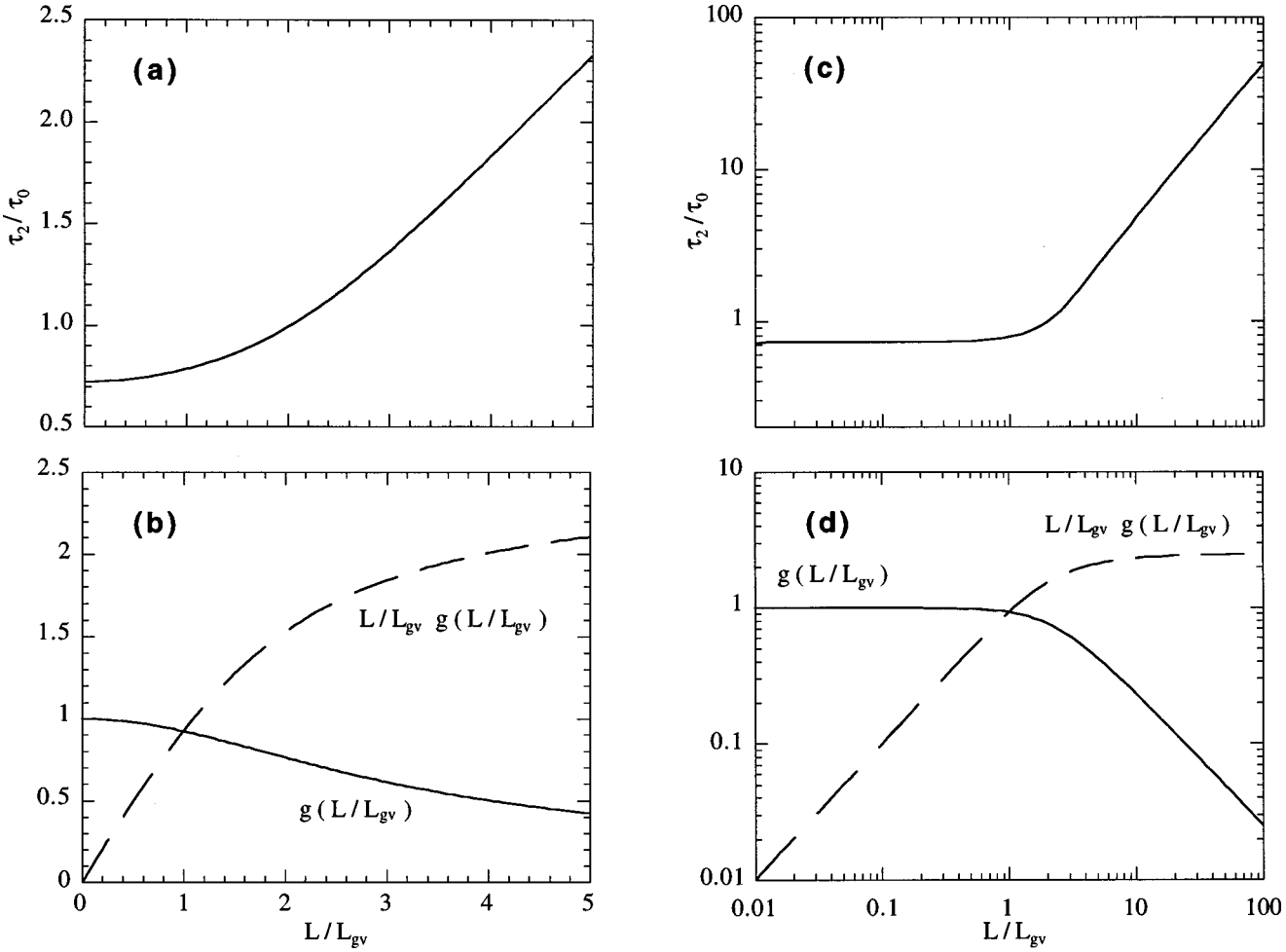

Fig. 3. (a), (c), normalized 1/*e* power half-width of a SH pulse, τ_2/τ_0, generated with a uniform grating of length L, as obtained from Eq. (39) for a Gaussian FH pulse of the form of Eq. (37). (b), (d), the efficiency-reduction factor, g, Eq. (64) (solid curves), and the $(L/L_{gv})g(L/L_{gv})$ factor (dashed curves). τ_2/τ_0, g, and $L/L_{gv}\,g(L/L_{gv})$ are plotted as functions of L/L_{gv} on linear [(a) and (b)] and logarithmic [(c) and (d)] scales.

With increasing L/L_{gv}, the SH pulse broadens, as seen in Figs. 3(a) and 3(c), owing to the walk-off effect. In the highly nonstationary limit, $L \gg L_{gv}$, the SH pulse has a top-hat profile and its half-width scales linearly with the crystal length, $\tau_2 \approx \delta\nu L/2$.[3,4,7–9] In the frequency domain this limit is equivalent to $\Delta\Omega_g \ll \Delta\Omega$. The spectrum of the SH is represented by the sinc factor in Eq. (39), so the FH pulse shape has little effect on the SH pulse shape in this limit.

6. NONUNIFORM QUASI-PHASE-MATCHING GRATINGS AND PULSE SHAPING

Let us consider a square nonuniform QPM grating whose variations in the local period $\Lambda(z)$ and in the local duty cycle $G(z)$ are slow, such that $d(z)$ can still be accurately represented as a sum of distinct Fourier components $d_m(z)$, as in Eq. (31), but with z-dependent amplitude and k vector. In this case the general form of $d_m(z)$ can be written as

$$d_m(z) = |d_m(z)|\exp[iK_{0m}z + i\Phi_m(z)], \qquad (41)$$

where we explicitly factored out the linear component of the total phase of the grating, $K_{0m}z$. Any desired phase of the grating, $\Phi_m(z)$, beyond the $K_{0m}z$ component, can be obtained by choice of the local k vector of the grating, $K_m(z) = 2\pi m/\Lambda(z)$, as

$$K_m(z) = K_{0m} + \frac{d\Phi_m}{dz}. \qquad (42)$$

$|d_m(z)|$ in Eq. (41) is the amplitude of the mth Fourier component of the grating, so an effectively continuous modulation of $|d_m(z)|$ can be engineered by variation of the local duty cycle of the grating, as in Eq. (32), where the duty cycle is now changing with z, $G = G(z)$.

Engineerability of $d_m(z)$ establishes the grounds for fairly general pulse shaping with QPM gratings. Indeed, given the temporal shape of the FH pulse, $E_1(t)$, and the desired shape of the SH pulse, $E_2(t)$, corresponding frequency-domain envelopes, $\widehat{A_1^2}(\Omega)$ and $\hat{A}_2(\Omega)$, respectively, are obtained by the Fourier transform. The transfer function $\hat{D}(\Omega)$, necessary to generate the desired $E_2(t)$, is then calculated from Eq. (26) as

$$\hat{D}(\Omega) = \frac{\hat{A}_2(\Omega)}{\widehat{A_1^2}(\Omega)}. \tag{43}$$

The required spatial distribution of the nonlinear coefficient, $d(z)$, necessary for a particular shaping function can be formally calculated from $\hat{D}(\Omega)$, obtained with Eq. (43), by the inverse Fourier transform of Eq. (25):

$$d(z) = i\frac{\delta\nu}{2\pi\gamma}\exp(i\Delta k_0 z)\int_{-\infty}^{+\infty}\frac{\hat{A}_2(\Omega)}{\widehat{A_1^2}(\Omega)}\exp(i\Omega\,\delta\nu z)\mathrm{d}\Omega. \tag{44}$$

We assume that the FH pulse spectrum overlaps the transfer function in a region owing to only one order of the QPM grating, i.e., $|\delta\nu\Omega| \ll K_{m+1} - K_m = K_1$ for all values of Ω for which $\widehat{A_1^2}(\Omega)$ has nonnegligible magnitude. In this case a physical QPM grating can then be synthesized such that its appropriate component $d_m(z)$ is equal to the mathematically formal $d(z)$ calculated with Eq. (44), and hence it will perform the desired transformation of $E_1(t)$ into $E_2(t)$.

We note that $d_m(z)$ is limited from above by the nonlinear susceptibility of the medium. Therefore the amplitude of $\hat{A}_2(\Omega)$ in Eq. (44), and hence the amplitude of the desired $E_2(t)$, cannot be arbitrarily high for a given $\widehat{A_1^2}(\Omega)$ and is in fact limited by the requirement that $|d(z)| \leqslant 2d_{\mathrm{eff}}/\pi m$. We also note that the transfer-function relation, Eq. (26), does not set a limit on the bandwidth of the generated SH. However, because a QPM grating acts like a passive filter on $\widehat{A_1^2}(\Omega)$, not an amplifier, the bandwidth of the SH pulse cannot exceed the bandwidth available from the FH, at least not without significant efficiency reduction. Therefore the shortest temporal feature of the shaped SH that can be obtained, δt, is inversely related to the bandwidth, $\Delta\Omega$, available from $\widehat{A_1^2}(\Omega)$, i.e., $\delta t \propto 1/\Delta\Omega$, with the proportionality constant being of the order of unity and its exact value depending on the shape of the pulses. The maximum possible temporal window T (or the best spectral resolution $\delta\Omega \propto 1/T$) of the shaper is determined by the length L of the device, i.e., $T = \delta\nu L$.

7. CHIRPED QUASI-PHASE-MATCHING GRATINGS AND PULSE COMPRESSION

As a particular example of general pulse shaping, in this section we discuss in more detail pulse compression with chirped QPM gratings. Let us consider a square, constant-duty-cycle, linearly chirped QPM grating whose k vector changes linearly with z, and hence the relevant component of whose spatial distribution of the nonlinear coefficient can be written in the form

$$d_m(z) = |d_m|\exp[iK_{0m}(z - L/2) + iD_g(z - L/2)^2] \times \mathrm{rect}(z/L - 1/2), \tag{45}$$

where $|d_m|$ is defined by Eq. (32), D_g is the grating chirp coefficient and $\mathrm{rect}(x)$ is a function defined such that $\mathrm{rect}(x) = 1$ for $|x| \leqslant 1/2$ and $\mathrm{rect}(x) = 0$ otherwise. This form of $d_m(z)$ is chosen such that at the center of the grating, $z = L/2$, the z-dependent phase of the grating, $\Phi_m(z)$, defined in Eq. (41), equals zero and the z-dependent k vector of the grating, $K_m(z)$, equals the carrier k vector K_{0m}. The transfer function for this grating can be calculated with Eq. (25) as

$$\hat{D}(\Omega) = \gamma|d_m|\int_{-L/2}^{+L/2}\exp[-i(\Delta k_0 - K_{0m} + \delta\nu\Omega)z + iD_g z^2]\mathrm{d}z, \tag{46}$$

where we neglect a linear-in-Ω phase factor.

We recognize the integral in Eq. (46) as the well-known Fresnel integral. When the bandwidth of the tuning curve exceeds the bandwidth of $\widehat{A_1^2}(\Omega)$, Eq. (46) can be accurately approximated over the spectrum of the pulse by the asymptotic form for an infinitely long crystal, resulting in

$$\hat{D}(\Omega) = \gamma|d_m|\sqrt{\frac{\pi}{D_g}}\exp\left(-i\frac{\delta\nu^2\Omega^2}{4D_g}\right), \tag{47}$$

where we assumed $K_{0m} = \Delta k_0$. The form of Eq. (47) suggests an analogy between the chirp rate of the QPM grating, D_g, and GVD. Independent of the input FH pulse shape, the SH experiences an additional effective GVD relative to the FH of $\delta\nu^2/2D_g$ and therefore can be compressed or stretched relative to the FH pulse.

As an example, we discuss the effect of the transfer function of Eq. (47) on a chirped Gaussian input pulse. We assume an input pulse that was created by dispersion of a transform-limited Gaussian pulse of the form of Eq. (37) in a linear delay line with GVD of C_1. The time-domain envelope of the electric field that corresponds to this pulse is

$$B_1(0,t) = E_0\frac{\tau_0}{\sqrt{\tau_0^2 + iC_1}}\exp\left[-\frac{t^2}{2(\tau_0^2 + iC_1)}\right], \tag{48}$$

and its $1/e$ power half-width is

$$\tau_1 = \sqrt{\tau_0^2 + (C_1/\tau_0)^2}. \tag{49}$$

Using the frequency-domain envelope definition, Eq. (10), we obtain $\hat{A}_1(\Omega)$ for this pulse as

$$\hat{A}_1(\Omega) = \frac{1}{\sqrt{2\pi}}E_0\tau_0\exp\left[-\frac{1}{2}(\tau_0^2 + iC_1)\Omega^2\right]. \tag{50}$$

Substituting Eqs. (47) and (50) into Eq. (26), we obtain the output SH envelope generated in the chirped grating:

$$\hat{A}_2(L,\Omega) = \frac{1}{2}\gamma|d_m|E_0^2\frac{1}{\sqrt{D_g}}\frac{\tau_0^2}{\sqrt{\tau_0^2 + iC_1}} \times \exp\left[-\frac{1}{2}(\tau_0^2/2 + iC_2)\Omega^2\right], \tag{51}$$

where C_2 is the chirp of the SH pulse:

$$C_2 = \frac{1}{2}(C_1 + \delta\nu^2/D_g). \tag{52}$$

Finally, by the inverse Fourier transform we find the time-domain SH envelope as

$$B_2(L,t) = \gamma|d_m|E_0^2\sqrt{\frac{\pi}{D_g\tau_1}}\,\tau_0\sqrt{\frac{\tau_0^2 - iC_1}{\tau_0^2 + i2C_2}} \times \exp\left[-\frac{t^2}{2(\tau_0^2/2 + iC_2)}\right], \tag{53}$$

where we neglect a constant shift in time of the pulse as a whole. We note that the chirp of the SH pulse depends on the chirp of the FH pulse and the chirp of the QPM grating. The length of the SH pulse is given by

$$\tau_2 = \sqrt{(\tau_0\sqrt{2})^2 + (\sqrt{2}C_2/\tau_0)}. \tag{54}$$

If the QPM grating is designed such that

$$D_g = D_g^{\mathrm{opt}} \equiv -\frac{\delta\nu^2}{C_1}, \tag{55}$$

then the SH pulse has no chirp, $C_2 = 0$; i.e., it is transform limited and the chirp on the input FH pulse has been compensated by the QPM grating. In this case the SH is given, to within a constant phase factor, by

$$B_2(L,t) = E_2\exp\left(-\frac{t^2}{\tau_0^2}\right), \tag{56}$$

where the amplitude of the generated SH wave is

$$E_2 = \gamma|d_m|\sqrt{\frac{\tau_0}{\tau_1}}\,\frac{\sqrt{\pi C_1}}{\delta\nu}E_0^2. \tag{57}$$

The results of Eqs. (49) and (54) are plotted in Fig. 4, which shows pulse lengths of the input chirped FH pulse, τ_1, and the generated SH pulse, τ_2, both normalized to τ_0, as functions of the normalized input FH chirp C_1/τ_0^2. In this figure we take the normalized grating chirp $D_g(\tau_0/\delta\nu)^2 = -0.1$. As can be seen in Fig. 4, when the FH pulse is chirped with $C_1/\tau_0^2 = 10$, the chirp of the SH pulse is zero, in accord with Eq. (52); i.e., the SH is compressed and its length is $\tau_2 = \tau_0/\sqrt{2}$. The relative shift

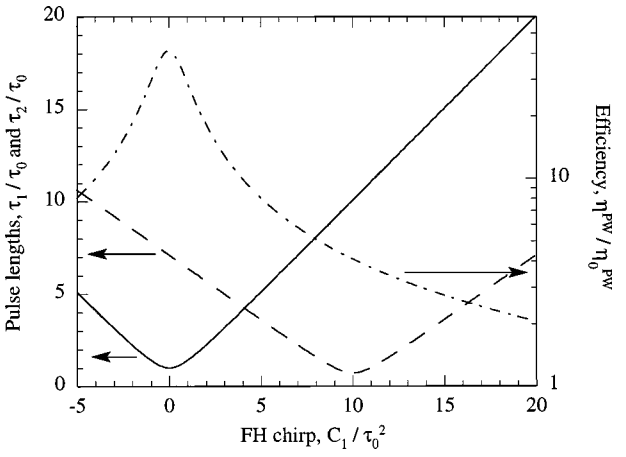

Fig. 4. Normalized FH pulse length, τ_1/τ_0 [solid curve, Eq. (49)], normalized SH pulse length, τ_2/τ_0 [dashed curve, Eq. (54)], and normalized plane-wave efficiency, η^{PW}/η_0^{PW} [dash-dotted line, Eq. (69)], plotted as functions of normalized FH chirp, C_1/τ_0^2. A chirped grating with a normalized chirp $D_g(\tau_0/\delta\nu)^2 = -0.1$ is assumed.

of the pulse-duration curves for the FH and the SH represents the effective GVD of the chirped QPM grating.

In deriving Eq. (47) we assumed that the chirped grating was long enough that its acceptance bandwidth, i.e., the width $\Delta\Omega_g$ of $\hat{D}(\Omega)$ given by Eq. (46), was greater than that of $\widehat{A_1^2}(\Omega)$. The dependence of the bandwidth of a chirped grating with a fixed D_g on the grating length requires further elaboration. Equation (46) can be rewritten as

$$\hat{D}(\Omega) = \gamma|d_m|\sqrt{\frac{\pi}{D_g}}\exp\left(-i\frac{\delta\nu^2\Omega^2}{4D_g}\right)F(\Omega), \tag{58}$$

with

$$F(\Omega) = \frac{1}{\sqrt{\pi}}\int_{x_0-X}^{x_0+X}\exp(ix^2)\mathrm{d}x, \tag{59}$$

where we defined dimensionless parameters $x_0 = -(\delta\nu\Omega)/(2\sqrt{D_g})$ and $X = \sqrt{D_g}L/2$. For a given D_g, x_0 serves as a normalized frequency, and X serves as a normalized crystal length. In Eq. (58) we explicitly factored out the desired quadratic phase factor; the Fresnel integral $F(\Omega)$ defined by Eq. (59) represents a correction owing to finite crystal length. For a given D_g and large enough L, such that $X \gg 1$ and $X \gg x_0$, Eq. (58) indeed reduces to Eq. (47). Figure 5 shows representative Fresnel integrals $F(\Omega)$ as a function of x_0 for different values of X. For $X \geqslant 5$ the amplitude of $F(\Omega)$ has a characteristic top-hat shape with a bandwidth of $\Delta x_0 = 2X$, over which the phase of $F(\Omega)$ is essentially zero. The chirped grating bandwidth is then expressed in terms of the crystal length as

$$\Delta\Omega_g = \frac{2D_gL}{\delta\nu}. \tag{60}$$

We note that for a fixed D_g the grating bandwidth scales linearly with L. This expression can also be obtained by our taking the difference between local k vectors at the edges of the grating, $\Delta\Omega_g\delta\nu = K_m(z = L) - K_m(z = 0) = 2D_gL$.

Compared with the grating with large X, for small X ($X \leqslant 5$), $F(\Omega)$ has significant amplitude modulation over $|x_0| < X$ and, more importantly, more pronounced phase modulation. The simple relation between the bandwidth of the grating and its length, Eq. (60), does not hold in this regime. Given the tolerances on the amplitude and the phase modulation for a particular device, the appropriate length L can always be found with Eqs. (58) and (59) such that the grating has the desired bandwidth $\Delta\Omega_g$.

In the regime $X \gg 1$ the amplitude of $\hat{D}(\Omega)$ is essentially a top-hat function with width $\Delta\Omega_g$ given by Eq. (60). For a Gaussian FH pulse of the form of Eq. (50), however, $\widehat{A_1^2}(\Omega)$ has a Gaussian profile with the $1/e$ spectral intensity half-width of $\Delta\Omega = \sqrt{2}/\tau_0$, and spectral components outside of the $\pm\sqrt{2}/\tau_0$ frequency range carry nonnegligible spectral power. For fixed D_g, to accommodate conversion of all frequency components, the length L of the chirped grating has to be long enough such that $\Delta\Omega_g$ is substantially broader than $\Delta\Omega$. However, as we will see later, for confocal focusing with Gaussian beams, the effi-

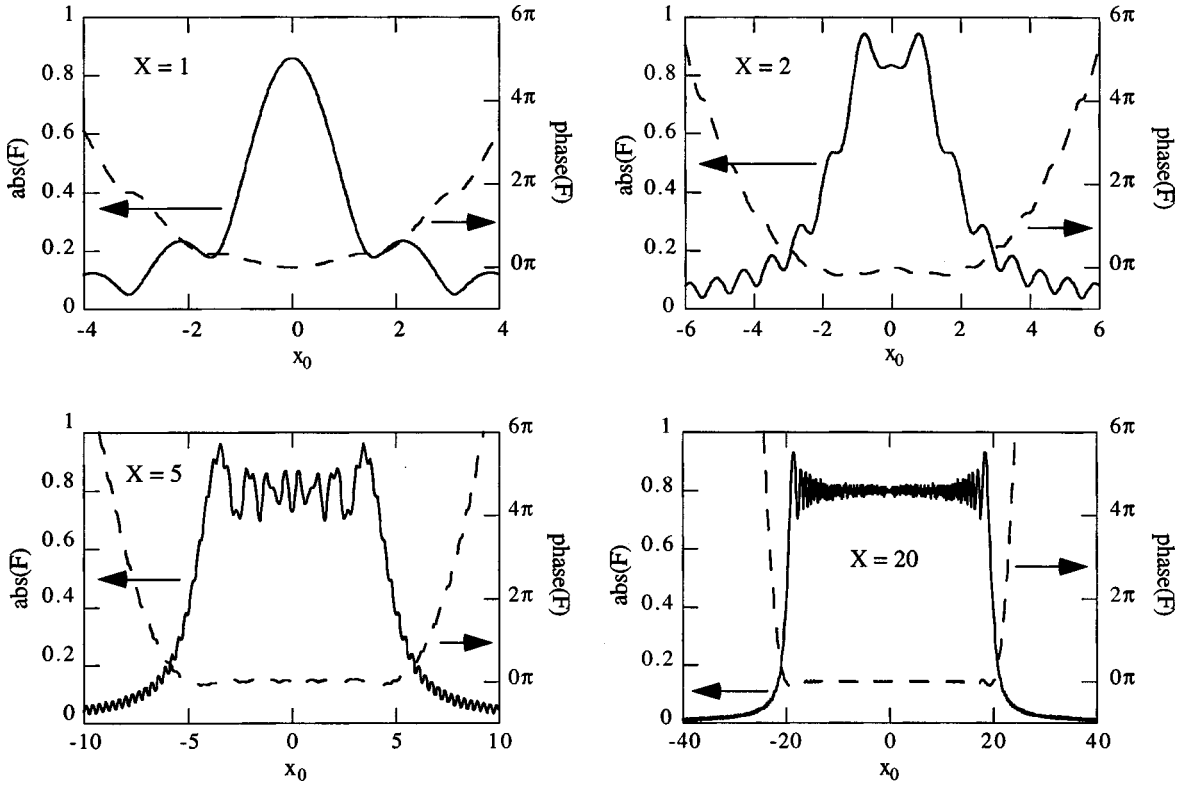

Fig. 5. Absolute value (solid curves) and phase (dashed curves) of representative integrals $F(\Omega)$, defined by Eq. (59), as a function of x_0 for different values of X.

ciency scales inversely with L, and hence a compromise between bandwidth matching and efficiency has to be made.

If L is selected such that $\Delta\Omega_g$ is comparable to $\sqrt{2}/\tau_0$, the grating will effectively truncate the SH frequency components Ω outside of the $|\Omega| \leqslant \Delta\Omega_g/2$ range, which would have been generated in the grating of infinite length. This spectral truncation leads to pulse broadening in the time domain as well as to some efficiency reduction. To quantify the problem we assume that the amplitude of $\hat{D}(\Omega)$ is a top-hat function with bandwidth of the form $\Delta\Omega_g = N/\tau_0$ and compute the resulting SH pulse temporal profile as a function of N. Figure 6 shows the $1/e$ temporal power half-width of the compressed SH pulse and the SH pulse energy, both normalized to the respective values that can be obtained with a grating of infinite length. As can be seen, for $N > 6$ the relative pulse broadening owing to the spectral truncation is less than 10%, and energy lost is less than 1%. Depending on the tolerances an appropriate N can be selected with Fig. 6. The necessary grating length can then be obtained with Eq. (60) as

$$L = \frac{N}{2}\frac{\delta\nu}{D_g\tau_0}. \tag{61}$$

For a grating designed to generate a compressed SH pulse, $D_g = D_g^{\mathrm{opt}}$, as defined in Eq. (55), the condition $X \gg 1$ is equivalent to the FH pulse being strongly chirped, i.e., $C_1 \gg \tau_0^2$, and hence from Eq. (49), $\tau_1 \approx |C_1|/\tau_0$. Equation (61) can then be rewritten as

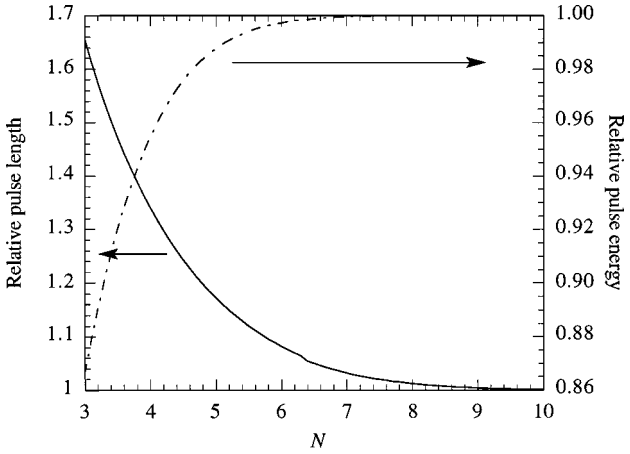

Fig. 6. Effect of bandwidth truncation by a chirped grating of finite length $L = N\delta\nu/(2D_g\tau_0)$ on the SH pulse $1/e$ power half-width (solid curve) and output energy (dash-dotted curve). Both are normalized to respective values obtained with a grating of infinite length and plotted as functions of N.

$$L = \frac{N}{2}\frac{\tau_1}{\delta\nu}, \tag{62}$$

In the time domain, Eq. (62) can be interpreted as that the SH pulse has to walk through in time over the central $N\tau_1/2$ part of the FH pulse for frequency components of the chirped FH pulse to be converted into the SH.

8. PLANE-WAVE EFFICIENCY SCALING

The energy-conversion efficiency is defined as the ratio of the energy of the generated SH pulse, U_2, to the FH

pulse energy, U_1. For plane waves the efficiency for a general QPM-SHG pulse shaper is obtained from the transfer-function relation, Eq. (26), by integration of the input FH and the output SH spectral intensities over all frequencies, resulting in

$$\eta^{\mathrm{PW}} \equiv \frac{U_2}{U_1} = \frac{n_2}{n_1} \frac{\int_{-\infty}^{+\infty} |D(\Omega)|^2 |\widehat{A_1^2}(\Omega)|^2 \mathrm{d}\Omega}{\int_{-\infty}^{+\infty} |\hat{A}_1(\Omega)|^2 \mathrm{d}\Omega}. \tag{63}$$

As can be seen from Eq. (63), the efficiency scaling for a general QPM-SHG shaper is a complicated function of the input FH spectrum and the particular shaping function. To derive the efficiency-scaling laws from Eq. (63) it is necessary to assume a particular class of shaping devices and a particular class of FH spectra. In the reminder of this section we will assume a Gaussian, possibly linearly chirped, FH pulse in the form of Eq. (50). Note that the scaling laws derived in this section are valid for other pulse shapes too, with small differences in the numerical factors.

Let us first consider the efficiency scaling for a uniform QPM grating, which has a transfer function given by Eq. (33). Assuming that the FH pulse is transform limited [Eq. (37)] and that the SHG process is quasi phase matched, $K_{0m} = \Delta k_0$, we obtain from Eq. (63)

$$\eta^{\mathrm{PW}} = 2\sqrt{2}\pi^2 \frac{|d_m|^2}{n_1 n_2 \lambda_1^2} E_0^2 L^2 g(L/L_{\mathrm{gv}}), \tag{64}$$

where the group-velocity walk-off length L_{gv} is defined by Eq. (40) and $g(L/L_{\mathrm{gv}})$ is the efficiency-reduction factor, shown in Figs. 3(b) and 3(d), as obtained by numerical integration of Eq. (63). For the quasi-stationary case, when the walk-off effects can be neglected, i.e., when $L \ll L_{\mathrm{gv}}$, the efficiency reduction factor $g = 1$; hence the efficiency scales with L^2 and Eq. (64) gives the quasi-cw energy-efficiency expression for a long Gaussian pulse. For the highly nonstationary case, i.e., when $L \gg L_{\mathrm{gv}}$, asymptotic evaluation of the integral in Eq. (63) shows that $g = \sqrt{2\pi} L_{\mathrm{gv}}/L$, and hence the efficiency scales linearly with crystal length.[9] However, the SH pulse length also increases linearly with crystal length, as discussed in Section 5 and shown in Fig. 3. From Fig. 3 it appears that a reasonable compromise between the efficiency and the SH pulse length is to use a crystal with length $L_{\mathrm{opt}} = 2L_{\mathrm{gv}}$: the SH pulse length is equal to that of the FH and $g(L/L_{\mathrm{gv}} = 2) = 0.764$. For such a crystal the efficiency is obtained from Eq. (64) as

$$\eta_0^{\mathrm{PW}} = 21.3 \frac{|d_m|^2}{n_1 n_2 \lambda_1^2} E_0^2 L_{\mathrm{gv}}{}^2. \tag{65}$$

As a second example we consider a pulse shaper whose acceptance bandwidth, $\Delta\Omega_g$, is much narrower than the bandwidth of $\widehat{A_1^2}(\Omega)$, $\Delta\Omega$, such that we can replace $\widehat{A_1^2}(\Omega)$ with $\widehat{A_1^2}(\Omega = 0)$, which can then be factored out of the integral in the numerator of Eq. (63), resulting in

$$\eta^{\mathrm{PW}} = \frac{n_2}{n_1} \frac{|\widehat{A_1^2}(\Omega = 0)|^2 \int_{-\infty}^{+\infty} |\hat{D}(\Omega)|^2 \mathrm{d}\Omega}{\int_{-\infty}^{+\infty} |\hat{A}_1(\Omega)|^2 \mathrm{d}\Omega}. \tag{66}$$

The integral in the numerator of Eq. (66) is proportional to the area under the tuning curve. According to Parseval's theorem and Eq. (25), defining $\hat{D}(\Omega)$, this area can be expressed as

$$\int_{-\infty}^{+\infty} |\hat{D}(\Omega)|^2 \mathrm{d}\Omega = \frac{2\pi\gamma^2}{\delta\nu} \int_{-\infty}^{+\infty} |d(z)|^2 \mathrm{d}z = \frac{2\pi\gamma^2}{\delta\nu} fL \left(\frac{2 d_{\mathrm{eff}}}{\pi m} \right)^2, \tag{67}$$

where the second equality in Eq. (67) implicitly defines the grating fill factor, f. Note that $f = 1$ for a grating with a constant duty cycle chosen to maximize $|d_m|$. We note that the area under the tuning curve is proportional to the grating length and does not depend on the details of the grating phase modulation, i.e., the grating k-vector distribution $K_m(z)$, as long as it gives the same fill factor f. Substituting Eq. (67) into Eq. (66) and evaluating it for a Gaussian pulse of the form Eq. (50), we obtain

$$\eta^{\mathrm{PW}} = \frac{\sqrt{2\pi}}{g(L/L_{\mathrm{gv}} = 2)} \frac{\delta\nu L}{\tau_1} f \eta_0^{\mathrm{PW}}, \tag{68}$$

where we explicitly factored out η_0^{PW} given by Eq. (65). As can be seen from Eq. (68), η^{PW} in the case when $\Delta\Omega_g$ is much narrower than $\Delta\Omega$ depends only on the material parameters and scales linearly with the crystal length and the peak power of the FH pulse, as represented by the factor $1/\tau_1$. All the grating properties are lumped into the single fill factor f in this efficiency expression.

For the chirped QPM grating the transfer function is given by Eq. (47) and the efficiency is obtained as

$$\eta^{\mathrm{PW}} = \frac{\pi}{g(L/L_{\mathrm{gv}} = 2)} \frac{\delta\nu^2}{D_g \tau_1 \tau_0} \eta_0^{\mathrm{PW}}. \tag{69}$$

We note that η^{PW} is independent of the crystal length, as long as the length is chosen according to Eq. (61) with $N > 6$, such that the chirped grating has enough bandwidth to accommodate the conversion of all frequency components. The scaling of the efficiency thus depends on which experimental parameters are held constant. If the chirp on the QPM grating, D_g, is fixed, η^{PW} scales with the peak intensity of the stretched FH pulse, as shown in Fig. 4, where $\eta^{\mathrm{PW}}/\eta_0^{\mathrm{PW}}$ is plotted in as a function of normalized FH chirp, C_1/τ_0^2. However, if the grating chirp is chosen to generate a compressed SH pulse, i.e., $D_g = D_g^{\mathrm{opt}}$ and the FH pulse is strongly chirped, $C_1 \gg \tau_0^2$, then Eq. (69) reduces to $\eta^{\mathrm{PW}} = 4.11\eta_0^{\mathrm{PW}}$, which no longer depends on the amount of stretching.

9. EFFICIENCY SCALING WITH FOCUSED BEAMS

Most applications require high efficiency and therefore confocal focusing of the FH beam in the nonlinear mate-

rial. We will include the effects of focusing into the efficiency calculations by generalizing the results of Boyd and Kleinman for cw SHG of Gaussian beams.[34] The plane-wave nonstationary efficiency described by general expression (63) is still applicable in the near-field limit. However, when the interaction occurs in neither the near-field nor the stationary limit, the focusing conditions and the temporal effects become coupled and lead to complicated efficiency expressions. With this caveat we will still treat the focusing and temporal effects independently, which allows a straightforward generalization of the Boyd and Kleinman results for cw SHG to the description of focused ultrashort-pulse SHG, and we obtain simple efficiency-scaling laws. We use the effective area of the FH beam for cw SHG, $S_{\mathrm{eff}} = L\lambda_1/4n_1h$, where h is the Boyd and Kleinman cw SHG focusing factor.[34] In this section we derive the energy efficiency for the same specific cases as in the previous section.

We define the confocal efficiency η^{conf} as the energy efficiency when the FH Gaussian beam is confocally focused and hence $h = 0.8$.[34] The confocal efficiency for a uniform grating is obtained from Eq. (64) as

$$\eta^{\mathrm{conf}} = \frac{8\pi\sqrt{2\pi}}{c\epsilon_0}\frac{|d_m|^2}{\delta\nu n_1 n_2 \lambda_1^3} U_1 \frac{L}{L_{\mathrm{gv}}} g(L/L_{\mathrm{gv}})h, \quad (70)$$

where we expressed the peak amplitude of the FH pulse in terms of its pulse energy and the pulse length, and the latter is incorporated into the factor L_{gv}, defined in Eq. (40); Figs. 3(b) and 3(d) show the factor $L/L_{\mathrm{gv}}\, g(L/L_{\mathrm{gv}})$ as a function of L/L_{gv}. In the quasi-stationary case, i.e., $L \ll L_{\mathrm{gv}}$, $g = 1$, and the confocal efficiency scales linearly with L.[9] In the highly nonstationary case when $L \gg L_{\mathrm{gv}}$, g approaches $\sqrt{2\pi}L_{\mathrm{gv}}/L$, and η^{conf} saturates, becoming independent of the crystal length.[9] From Fig. 3 it is clear that confocal focusing with a crystal of length of $L_{\mathrm{opt}} = 2L_{\mathrm{gv}}$ results in efficiency within a factor of 0.61 of the maximum available and generates SH pulses with negligible pulse broadening relative to the FH pulse. The confocal efficiency for the crystal of length L_{opt} is then

$$\eta_0^{\mathrm{conf}} = \frac{76.7}{\epsilon_0\lambda_1^3}\mathrm{FOM}U_1, \quad (71)$$

where the material figure of merit, FOM, is defined as

$$\mathrm{FOM} = \frac{|d_m|^2}{c\delta\nu n_1 n_2}. \quad (72)$$

The efficiency depends only on material properties, represented by the figure of merit, and the FH pulse energy.

For a general pulse shaper in the regime $\Delta\Omega_g \ll \Delta\Omega$ we obtain the energy efficiency from Eq. (68) as

$$\eta^{\mathrm{conf}} = \frac{\sqrt{2\pi}}{g(L/L_{\mathrm{gv}} = 2)}\frac{\tau_0}{\tau_1} f\eta_0^{\mathrm{conf}}. \quad (73)$$

We note that this confocal efficiency is independent of the crystal length and the grating-modulation parameters other than the fill factor f. The important distinction between the filtering action of a QPM grating and that of a conventional linear band-pass filter is that the latter rejects energy outside of the pass band, whereas for the former the energy efficiency is independent of $\Delta\Omega_g$.

For a chirped grating the efficiency for the confocal focusing case is obtained from Eq. (69) as

$$\eta^{\mathrm{conf}} = \frac{2\pi}{g(L/L_{\mathrm{gv}} = 2)}\frac{\tau_0}{\tau_1}\frac{1}{N}\eta_0^{\mathrm{conf}}, \quad (74)$$

where we assume that the crystal length is given by Eq. (61) and that the SH pulse energy loss owing to spectral truncation is negligible. Thus in the confocally focused case, η^{conf} scales with the peak intensity of the stretched FH pulse and therefore, for fixed pulse energy, inversely with the stretching ratio, τ_0/τ_1. The factor $1/N$ in Eq. (74) represents the scaling of η^{conf} with the chirped grating length, $L \propto N$ from Eq. (61). Selecting $N = 6$ as a reasonable compromise between efficiency and pulse length (Fig. 6), we obtain that the chirped-grating case suffers an efficiency reduction of $0.69\tau_0/\tau_1$, as compared with the optimized unchirped case.

It is interesting to note that as long as the chirped grating has an adequate acceptance bandwidth, i.e., for a given D_g the grating length is selected according to Eq. (61), η^{conf} is independent of the grating chirp, and hence given the amount of FH stretching, the SH will be generated with the same efficiency for compressed or chirped SH pulses.

Many important laser systems that may be used as pump sources for the pulse-compression process analyzed above have the property of being peak-power limited. With such sources the pulse energy increases linearly with pulse duration and therefore increases linearly with stretching for a fixed bandwidth. Thus, if we consider the result of Eq. (74), SHG of such sources has an energy-conversion efficiency that is independent of stretching. A more detailed discussion of efficiency scaling appears in Ref. 26.

10. COMPARISON OF QUASI-PHASE-MATCHING MATERIALS

We now consider several technologically important QPM materials in the context of ultrashort-pulse SHG. Table 1 lists key parameters for SHG of the FH at wavelengths 1.56 μm and 800 nm in periodically poled lithium niobate (PPLN), lithium tantalate (PPLT), potassium niobate (PPKN), potassium titanyl phosphate (PPKTP), and rubidium titanyl arsenate (PPRTA). d_{33} is the largest element of the tensor of nonlinear coefficients for all materials considered here, and hence the first-order ($m = 1$) modulation of d_{33} gives the largest possible QPM nonlinearity, $(2/\pi)d_{33}$, as obtained from Eq. (32) by substitution of d_{33} for d_{eff}. All materials in Table 1 have comparable nonlinearities that are at least an order of magnitude higher than that of conventional birefringently phase-matched interactions, except for potassium niobate whose d_{31} is comparable to d_{33}.

The GVM parameter $\delta\nu$ is critical for spectral and temporal performance of a SHG device. For a fixed length of the crystal, $\delta\nu$ determines the available amount of group delay between FH and SH, and hence determines the longest temporal window in a QPM-SHG pulse shaper, $T = \delta\nu L$ (as discussed in Section 6), and therefore the maximum possible compression ratio in a chirped QPM

Table 1. Comparison of Nonlinear Coefficient, GVM Parameter, Figure of Merit, and Confocal Efficiency for Several QPM Materials

		$\delta\nu$, ps/mm		FOM, pm^2/V^2		η_0^{conf}, %/nJ	
Material	d_{33}, pm/V	1.56 μm	800 nm	1.56 μm	800 nm	1.56 μm	800 nm
PPLN[35]	27	0.30	1.90	708	102	162	173
PPLT[36]	15	0.25	1.53	270	40	61	68
PPKN[37]	27	0.32	2.40	680	83	155	140
PPKTP[38]	17	0.20	1.64	572	65	131	111
PPRTA[39]	16	0.24	1.73	405	52	92	88

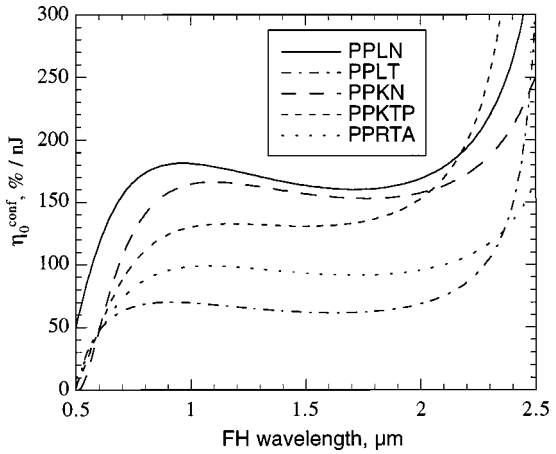

Fig. 7. SHG conversion efficiency η_0^{conf} as a function of the FH wavelength for representative first-QPM-order materials.

grating, as can be obtained from Eq. (62): $\tau_1/\tau_0 = \delta\nu L/2\tau_0$. Therefore for applications that require large group delays, it is advantageous to have large $\delta\nu$. The GVM parameter is highly dispersive and increases for shorter wavelengths. Because the maximum length of available QPM materials is of the order of several centimeters, the maximum group delay is in the range of 20 to 100 ps, which depends on the wavelength and the material used.

From the standpoint of achieving the highest possible efficiency, having a large GVM parameter is disadvantageous because the material figure of merit for ultrashort-pulse SHG, defined by Eq. (72), scales inversely with $\delta\nu$. Among the materials considered here, PPLN has the best FOM because of its high nonlinearity and relatively low $\delta\nu$. The FOM determines the confocal efficiency η_0^{conf} of a uniform grating with optimum length, Eq. (71), and hence the confocal efficiency of all devices considered in this paper, Eqs. (70), (73), and (74). For a given material and FH wavelength, η_0^{conf} scales linearly with the FH pulse energy and hence can be normalized to energy and can be expressed in units of % $\times$ (energy)$^{-1}$. Figure 7 shows such normalized η_0^{conf} as a function of wavelength for all QPM materials considered here. It is interesting to note that the material dispersion nearly cancels the explicit $1/\lambda_1^3$ dependence of η_0^{conf}, Eq. (71), resulting in a fairly constant efficiency over the visible to the near-infrared spectral region. We note, however, that the two-photon absorption of the SH can be significant in the wavelength region accessible with Ti:sapphire lasers ($\sim$800 nm) because of the high peak power of ultrashort pulses, and consequently the efficiencies shown in Fig. 7 may not be attainable in this spectral region.

11. SUMMARY AND FURTHER DIRECTIONS

In summary, we described a theory of SHG with longitudinally nonuniform QPM gratings in the undepleted-pump approximation. The use of frequency-domain envelopes with frequency-dependent k vectors allowed a simple derivation of the output SH field in the presence of arbitrary material dispersion. Neglecting GVD and higher-order dispersion, we obtained a transfer-function relationship describing the SHG process. This SHG transfer function depends only on material properties and on the QPM grating design. We showed that engineerability of the QPM gratings, and hence of the transfer function, is a basis for generation of nearly arbitrarily shaped SH pulses. We analyzed in detail a technologically important example of pulse shaping, the generation of compressed SH pulses from linearly chirped FH input pulses. We also derived the efficiency-scaling laws for several types of SHG devices.

In highly dispersive materials, or with wide-bandwidth FH fields, the simple transfer-function relation may no longer be accurate because it neglects GVD and higher-order dispersion at both FH and SH frequencies. Because dispersion is larger at shorter wavelengths, the GVD parameter at the SH is typically several times larger than that at the FH. It turns out that GVD and higher-order dispersion at the SH can straightforwardly be incorporated into the transfer-function description and are accounted for by appropriate choice of the k vector and/or the duty cycle of the grating. To the first order, GVD at the SH leads to the extra chirp of $\beta_2 L$ on the SH, and a linearly chirped grating can still be used for compression; however, its chirp D_g^{opt} should be selected as $D_g^{\text{opt}} = -\delta\nu^2/(C_1 + \beta_2 L)$, rather than D_g^{opt} given by Eq. (55). Inclusion of the GVD at the FH leads to a non-transfer-function expression for the SH. However, for a given FH pulse shape, GVD still can be accounted for in the design of the QPM grating. For example, a QPM grating required for pulse compression in the presence of GVD has a chirp that is nonlinear with length. The details of this study will appear in a subsequent paper.

Inclusion of pump depletion is important for understanding the limitations it imposes in the high-conversion-efficiency regime. Our preliminary numerical studies indicate that the cascaded phase shifts associated

with the back reaction of the SH on the FH can be important, but that for compression in gratings of optimal length, conversion approaching 50% with performance similar to the low-conversion case is possible.[40] Further work is necessary to clarify the limitations.

ACKNOWLEDGMENTS

This research was supported by Defense Advanced Research Projects Agency grant N00014-92-J-1903 through the Center for Nonlinear Optical Materials at Stanford University and the Joint Services Electronics Program through Stanford University/Office of Naval Research grant N00014-91-J-1050. G. Imeshev and M. A. Arbore acknowledge support from IMRA America.

*Present address: Lightwave Electronics, 2400 Charleston Road, Mountain View, California 94043.

REFERENCES

1. R. L. Byer, "Quasi-phasematched nonlinear interactions and devices," J. Nonlinear Opt. Phys. Mater. **6**, 549–592 (1997), and references therein.
2. S. L. Shapiro, "Second harmonic generation in $LiNbO_3$ by picosecond pulses," Appl. Phys. Lett. **13**, 19–21 (1968).
3. J. Comly and E. Garmire, "Second harmonic generation from short pulses," Appl. Phys. Lett. **12**, 7–9 (1968).
4. W. H. Glenn, "Second harmonic generation by picosecond optical pulses," IEEE J. Quantum Electron. **QE-5**, 284–290 (1969).
5. S. A. Akhmanov, A. P. Sukhorukov, and A. S. Chirkin, "Nonstationary phenomena and space–time analogy in nonlinear optics," Sov. Phys. JETP **28**, 748–757 (1969).
6. S. A. Akhmanov, A. I. Kovrygin, and A. P. Sukhorukov, in *Quantum Electronics: A Treatise*, H. Rabin and C. L. Tang, eds. (Academic, New York, 1975), Vol. 1.
7. S. A. Akhmanov, V. A. Vysloukh, and A. S. Chirkin, *Optics of Femtosecond Laser Pulses* (American Institute of Physics, Melville, New York, 1992).
8. A. M. Weiner, "Effect of group velocity mismatch on the measurement of ultrashort optical pulses via second harmonic generation," IEEE J. Quantum Electron. **QE-19**, 1276–1283 (1983).
9. A. M. Weiner, A. M. Kan'an, and D. E. Leaird, "High-efficiency blue generation by frequency doubling of femtosecond pulses in a thick nonlinear crystal," Opt. Lett. **23**, 1441–1443 (1998).
10. E. Sidick, A. Knoesen, and A. Dienes, "Ultrashort-pulse second harmonic generation in quasi-phase-matched dispersive media," Opt. Lett. **19**, 266–268 (1994).
11. E. Sidick, A. Knoesen, and A. Dienes, "Ultrashort-pulse second harmonic generation. I. Transform-limited fundamental pulses," J. Opt. Soc. Am. B **12**, 1704–1712 (1995).
12. E. Sidick, A. Knoesen, and A. Dienes, "Ultrashort-pulse second harmonic generation. II. Non-transform-limited fundamental pulses," J. Opt. Soc. Am. B **12**, 1713–1722 (1995).
13. E. Sidick, A. Knoesen, and A. Dienes, "Ultrashort pulse second harmonic generation in quasi-phase-matched structures," Pure Appl. Opt. **5**, 709–722 (1996).
14. A. Knoesen, E. Sidick, and A. Dienes, in *Novel Optical Materials and Applications*, I.-C. Khoo, F. Simoni, and C. Umeton, eds. (Wiley, New York, 1997).
15. J. A. Armstrong, N. Bloembergen, and P. S. Pershan, "Interactions between light waves in a nonlinear dielectric," Phys. Rev. **127**, 1918–1939 (1962).
16. M. M. Fejer, G. A. Magel, D. H. Jundt, and R. L. Byer, "Quasi-phase-matched second harmonic generation: tuning and tolerances," IEEE J. Quantum Electron. **28**, 2631–2654 (1992).
17. T. Suhara and H. Nishihara, "Theoretical analysis of waveguide second-harmonic generation phase matched with uniform and chirped gratings," IEEE J. Quantum Electron. **26**, 1265–1276 (1990).
18. Y. Ishigame, T. Suhara, and H. Ishihara, "$LiNbO_3$ waveguide second-harmonic-generation device phase matched with a fan-out domain-inverted grating," Opt. Lett. **16**, 375–379 (1991).
19. M. L. Bortz, M. Fujimura, and M. M. Fejer, "Increased acceptance bandwidth for quasi-phasematched second harmonic generation in $LiNbO_3$ waveguides," Electron. Lett. **30**, 34–35 (1994).
20. K. Mizuuchi, K. Yamamoto, M. Kato, and H. Sato, "Broadening of the phase-matching bandwidth in quasi-phase-matched second-harmonic generation," IEEE J. Quantum Electron. **30**, 1596–1604 (1994).
21. K. Mizuuchi and K. Yamamoto, "Waveguide second-harmonic generation device with broadened flat quasi-phase-matched response by use of a grating structure with located phase shifts," Opt. Lett. **23**, 1880–1882 (1998).
22. M. Cha, "Cascaded phase shift and intensity modulation in aperiodic quasi-phase-matched gratings," Opt. Lett. **23**, 250–252 (1998).
23. M. H. Chou, K. R. Parameswaran, M. M. Fejer, and I. Brener, "Multiple channel wavelength conversion using engineered quasi-phase-matching structures in $LiNbO_3$ waveguides," Opt. Lett. **24**, 1157–1159 (1999).
24. M. A. Arbore, O. Marco, and M. M. Fejer, "Pulse compression during second-harmonic generation in aperiodic quasi-phase-matching gratings," Opt. Lett. **22**, 865–867 (1997).
25. M. A. Arbore, A. Galvanauskas, D. Harter, M. H. Chou, and M. M. Fejer, "Engineerable compression of ultrashort pulses by use of second-harmonic generation in chirped-period-poled lithium niobate," Opt. Lett. **22**, 1341–1343 (1997).
26. M. A. Arbore, "Generation and manipulation of infrared light using quasi-phasematched devices: ultrashort-pulse, aperiodic-grating and guided-wave frequency conversion," Ph.D. dissertation (Stanford University, Stanford, Calif., 1998).
27. A. Galvanauskas, D. Harter, M. A. Arbore, M. H. Chou, and M. M. Fejer, "Chirped-pulse-amplification circuits for fiber amplifiers, based on chirp-period quasi-phase-matching gratings," Opt. Lett. **23**, 1695–1697 (1998).
28. A. Galvanauskas, A. Hariharan, D. Harter, A. A. Arbore, and M. M. Fejer, "Microlaser pumped, engineerable bandwidth parametric chirped-pulse amplifier using electric-field-poled $LiNbO_3$," in *Conference on Lasers and Electro-Optics*, Vol. 6 of 1998 Technical Digest Series (Optical Society of America, Washington, D.C., 1998), p. 16.
29. P. Loza-Alvarez, D. T. Reid, P. Faller, M. Ebrahimzadeh, W. Sibbett, H. Karlsson, and F. Laurell, "Simultaneous femtosecond-pulse compression and second-harmonic generation in aperiodically poled $KTiOPO_4$," Opt. Lett. **24**, 1071–1073 (1999).
30. M. Hofer, M. E. Fermann, A. Galvanauskas, D. Harter, and R. S. Windeler, "Low-noise amplification of high-power pulses in multimode fibers," IEEE Photonics Technol. Lett. **11**, 650–652 (1999).
31. G. Imeshev, A. Galvanauskas, D. Harter, M. A. Arbore, M. Proctor, and M. M. Fejer, "Engineerable femtosecond pulse shaping by second-harmonic generation with Fourier synthetic quasi-phase-matching gratings," Opt. Lett. **23**, 864–866 (1998).
32. S. K. Kurtz, in *Quantum Electronics: A Treatise*, H. Rabin and C. L. Tang, eds. (Academic, New York, 1975).
33. G. P. Agrawal, *Nonlinear Fiber Optics*, 2nd ed. (Academic, San Diego, Calif., 1995).
34. G. D. Boyd and D. A. Kleinman, "Parametric interactions of focused Gaussian light beams," J. Appl. Phys. **39**, 3597–3639 (1968).
35. D. H. Jundt, "Temperature-dependent Sellmeier equation for the index of refraction, n_e, in congruent lithium niobate," Opt. Lett. **22**, 1553–1555 (1997).

36. J.-P. Meyn and M. M. Fejer, "Tunable ultraviolet radiation by second-harmonic generation in periodically poled lithium tantalate," Opt. Lett. **22**, 1214–1216 (1997).
37. B. Zysset, I. Biaggio, and P. Gunter, "Refractive indices of orthorhombic $KNbO_3$. I. Dispersion and temperature dependence," J. Opt. Soc. Am. B **9**, 380–386 (1992).
38. L. K. Cheng, L. T. Cheng, J. Galperin, P. A. Morris Hotsenpiller, and J. D. Bierlein, "Crystal growth and characterization of $KTiOPO_4$ isomorphs from the self-fluxes," J. Cryst. Growth **137**, 107–115 (1994).
39. D. L. Fenimore, K. L. Schepler, D. Zelmon, S. Kuck, U. B. Ramabadran, P. Von Richter, and D. Small, "Rubidium titanyl arsenate difference-frequency generation and validation of new Sellmeier coefficients," J. Opt. Soc. Am. B **13**, 1935–1940 (1996).
40. G. Imeshev, M. A. Arbore, A. Galvanauskas, and M. M. Fejer, "Numerical simulations of ultrafast SHG with chirped QPM gratings in the pump-depleted regime," Center for Nonlinear Optical Materials annual report (Stanford University, Stanford, Calif., 1997).